Eur. Phys. J. A **8**, 87–96 (2000)

THE EUROPEAN PHYSICAL JOURNAL A

On the spectroscopy of atomic electrons (positrons) in the energy range of 10 to 50 MeV from heavy-ion collisions at intermediate energies

K.E. Stiebing[1,a], K.A. Müller[1], J. Baumann[2], K. Bethge[1], J. Bernhardt[1], H. Bokemeyer[2], H. Folger[2], O. Fröhlich[1], O. Hohn[1], G. Kavermann[1], G. Lambrinidis[1], A. Müller[1], J. Peter[1], S. Runkel[1], L. Schmidt[1], H. Schmidt-Böcking[1], P. Senger[2], P. Thee[1], and J. Ullrich[2]

[1] Institut für Kernphysik der Johann Wolfgang Goethe-Universität, August-Euler-Str. 6, D-60486 Frankfurt/M., Germany
[2] Gesellschaft für Schwerionenforschung, Planckstr. 1, D-64291 Darmstadt, Germany

Received: 28 December 1999 / Revised version: 23 March 2000
Communicated by: D. Schwalm

Abstract. The feasibility of the spectroscopy of dynamically ionized electrons (positrons) from heavy-ion collisions at intermediate energies, *e.g.* Pb+Pb at 60 A·MeV has been studied. We propose a magnetic toroid spectrometer for lepton spectroscopy in an energy range between 5 and 50 MeV. Special emphasis was laid on large solid angles, on broad-band characteristics and on a good suppression of secondary events. The device is a versatile compact-size instrument for lepton detection in in-beam experiments at a moderate energy resolution of $\Delta E/E \approx 4\%$.

PACS. 07.81.+a Electron, ion spectrometers, and related techniques – 25.70.-z Low and intermediate energy heavy-ion reactions – 29.30.Aj Charged-particle spectrometers: electric and magnetic – 29.30.Ep Charged-particle spectroscopy

1 Introduction

The spectroscopy of primary electrons (positrons) ejected from ion-atom collisions is a direct way to provide information on the dynamical aspects of nuclear reactions and excitations as well as on the underlying stationary properties of the atomic or quasiatomic systems. In the regime of very heavy-ion-atom collisions at and slightly above Coulomb barrier energies the spectroscopy of dynamically ionized electrons (δ-electrons) and positrons has become a standard tool of experimental heavy-ion physics [1–5]. Of particular interest are electrons ejected from the strongest bound atomic shells or positrons from pair creation by ionization of levels of the continuum of negative energies [6–11]. Due to their high intrinsic momenta these leptons are emitted with kinetic momenta that exceed the maximum momentum transfer in elastic quasi-free collisions by orders of magnitude. They are therefore well separated by their energy from the other atomic ionization processes and represent unique probes for the study of quantum electrodynamics in extremely strong, transient fields. Basically, the shapes of these lepton spectra reflect the time dependence of the internuclear potential [11–14] and the spectroscopy of dynamical electrons or positrons may be used to provide information on the time evolution of the nuclear collision itself, serving as an "atomic clock" for the nuclear reaction [12]. This spectroscopy and its theoretical interpretation were major topics of research at the heavy-ion accelerator UNILAC of the Gesellschaft für Schwerionenforschung, GSI, Darmstadt, Germany [15–26]. With the heavy-ion synchrotron SIS at GSI (*e.g.*, [27]), a new range of projectile energies became accessible allowing to pursue these physics into the domain of relativistic ion velocities. There a breakdown of the so far very successful adiabatic coupled channel approach [28] is expected as soon as the electrons have not enough time to instantaneously adjust their movement to the time variation of the internuclear potential so that retardation effects have to be taken into account.

Extensions of the above theoretical approach to intermediate collision energies indicate [26,29–31], that the δ-electron spectra will extend to energies as high as 60 MeV with very low but experimentally accessible cross-sections in the order of 10 nb/MeV. In fig. 1 the predicted differential cross-sections for electron emission are given for collisions of 60 A·MeV Pb on Pb on the basis of a schematic collision model for various assumptions on the collision time [31]. For a detailed description of the theory and its derivation see the thesis of Th. de Reus [32].

For a study of the properties of nuclear matter in relativistic heavy-ion collisions, the beam energy range between 20 and 100 A·MeV (intermediate energy range) is of

[a] e-mail: Stiebing@ikf.uni-frankfurt.de

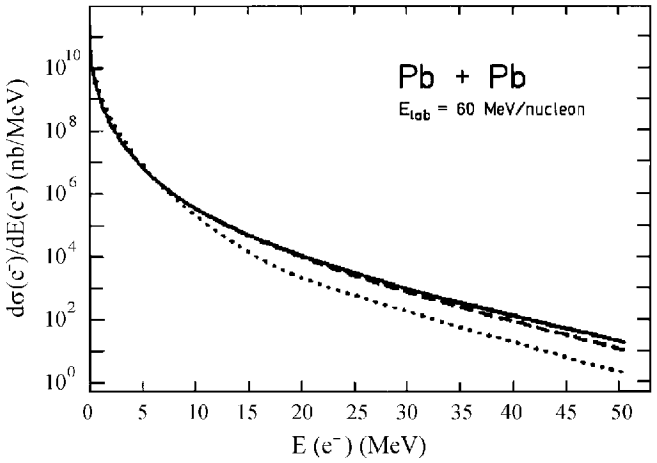

Fig. 1. δ-electron spectrum for Pb+Pb collisions integrated over impact parameters from b=0 to 14 fm for an intermediate collision energy of 60 A·MeV. The different distributions belong to collision times of 1.03×10^{-23}s (full line), 1.20×10^{-23}s (dashed) and 1.50×10^{-23}s (dotted) (from [31]).

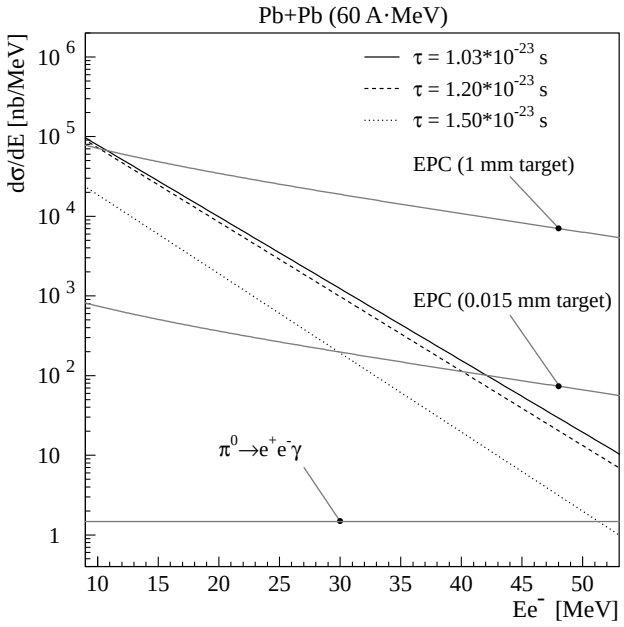

Fig. 2. Differential cross-sections in the energy range from 10 to 55 MeV for dynamic electron emission in comparison to various background processes (CM-system).

particular interest. Unexpectedly high production rates of pions at energies well below their nucleon-nucleon threshold [33,34] demand for cooperative processes during the first energy-dissipating phase of close nuclear encounters. Using leptons as electromagnetic probes has the attractive feature that, except for the Coulomb interaction, leptons are decoupled from the later development of the nuclear medium. Therefore, they exclusively provide information on the early stage of the collision, during which the centre-of-mass (CM) kinetic energy of the collision partners is dissipated into the inner degrees of freedom of the compound nucleus.

The dynamic atomic lepton production has to be observed in the environment of a copious electron background, induced by nuclear reactions, which, already at the Coulomb barrier, is an important contribution to the total lepton spectrum. At intermediate beam energies, the dominant background processes at distant collisions (with no nuclear overlap) are internal and external pair-conversion of γ-radiation emerging from the de-excitation of the different modes of Coulomb excited giant multipole resonances (GMR) [35,36] at excitation energies of typically up to 30 A·MeV. For close collisions (with nuclear overlap) the dominant sources for background are external pair creation (EPC) of nuclear γ-radiation created during the thermalisation of the hot reaction zone (fireball) and π^0-decay (see, *e.g.*, [37–39]), direct reaction products from fragmentation (heavy particles), charged pions (which pass through the spectrometer due to their long life time $c\tau = 7.8$ m [40]) and secondary decay products, *e.g.* neutral pions.

In fig. 2 the predicted differential cross-sections for the dynamic atomic lepton production [31] are given for the experimentally more relevant energy window between 10 and 50 MeV together with the most important background contributions, EPC and Dalitz decay of neutral pions. External pair conversion (EPC) of nuclear Bremsstrahlung radiation in the target is given for two different target thicknesses. Compared to this contribution, EPC in the mechanical components of the spectrometer can be minimized to become negligible [41] (see also sect. 4.2). Being a secondary process, EPC depends quadratically on the target thickness and can therefore be reduced by choosing thin targets and high beam currents. The calculations are based on a cross-section of 17 mb for the inclusive photon production, taking data measured with the "Two Arms Photon Spectrometer" (TAPS) at 60 A·MeV Kr+Ni collisions [42] and the scaling systematics of refs. [34,43]. For the thick target EPC amounts to approximately 10% of the total γ-yield.

Neutral pions decay inside the target ($c\tau = 25.1$ nm). The Dalitz decay, $\pi^0 \rightarrow \gamma e^+e^-$, has a branching ratio of 1.2% [40]. Being created by the same type of collision (with small impact parameters), this process cannot be separated from "atomic" lepton emission. The "pionic" lepton spectrum is expected to be symmetric around its maximum at about 30 MeV due to the fact that on the average the rest mass of the pion is equally divided between the e^+e^--pair and the photon in the Dalitz decay. For an estimate of the order of magnitude as given in fig. 2 it was assumed that the electron (positron) emission is in first order isotropic [44] with an essentially flat energy distribution ranging from zero energy up to $m_{\pi^0}c^2/2 = 67.5$ MeV. For the π^0 production a cross-section of 100 μb has been calculated, using the systematics given in Metag [43] (see also fig. 3). Pion creation in this collision energy range is subthreshold, significantly decreasing with decreasing collision energy. Systematic measurements at various beam energies thus give a handle to separate atomic lepton contributions from those originating from π-production.

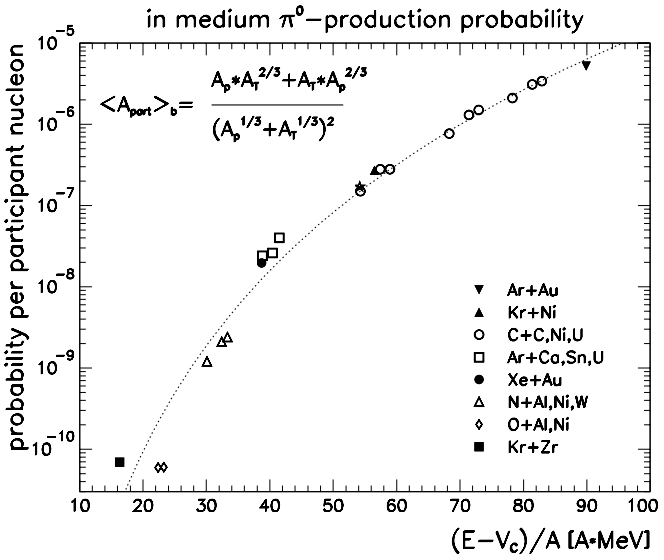

Fig. 3. π^0 emission probability as a function of the Coulomb-barrier reduced beam energy [43].

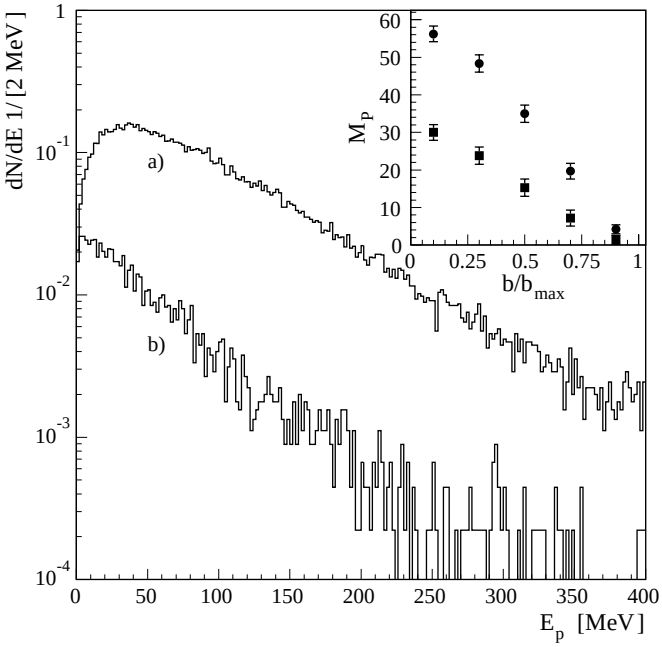

Fig. 4. Expected energy spectra for light charged particles ($Z = 1$) in the polar angular range between a) $10^\circ < \vartheta_{\rm lab} < 40^\circ$ and b) $110^\circ < \vartheta_{\rm lab} < 135^\circ$. The insert shows the expected multiplicity for light charged particle ($Z = 1$) as a function of the reduced impact parameter $b/b_{\rm max}$ emitted into a polar angular range of $0^\circ < \vartheta_{\rm lab} < 180^\circ$ (dots) and $10^\circ < \vartheta_{\rm lab} < 40^\circ$ (squares) with respect to the beam direction (FREESCO simulation). The average multiplicity for emission into the backward hemisphere $110^\circ < \vartheta_{\rm lab} < 135^\circ$ and $0 < b < b_{\rm max}$ is in the order of 1.

2 Basic considerations

2.1 Trigger on close collisions

The differential cross-sections for dynamically induced electron emission, displayed in fig. 1, have been integrated over a range of impact parameters b between complete nuclear overlap ($b = 0$ fm) and grazing collisions ($b = 14$ fm)[31]. For peripheral collisions ($b > 14$ fm) and at lepton energies beyond 10 MeV the cross-sections for the atomic process decrease to values that are no longer accessible by experiment. Here the "nuclear processes" (mainly Coulomb-excited GMR) become important. As the total (atomic and nuclear) emission cross-sections are dominated by the processes at large impact parameters ($\sigma_{\rm tot} = 2\pi \int b\, P(b)\, {\rm d}b$, $P(b)$ being the emission probability), a trigger on sufficiently close collisions is ultimately needed to exclude the contributions from nuclear excitation at distant collisions. This is best performed by a multiplicity measurement of heavy charged particles (p,d,α). In order to define the optimal position for such a detector we have carried out simulations with the code FREESCO [45]. The results of these calculations are summarized in fig. 4, where the energy spectra for light charged particles are displayed for the emission into a forward angular window (a) and a backward angular window (b) with respect to the lab. system. Here, for a clearer representation only the results for particles with $Z = 1$ are shown. The ratio of light charged particles amounts to p/d/t = 1:1:0.5 and ^{4}He/^{3}He = 8:1. The total ratio of charged particles with $Z = 1$ and $Z = 2$ was determined to be 3:1.

The ratio of ^{4}He/^{3}H is in good agreement with measurements of Milazzo *et al.* [46] in central 35 A·MeV Au + Au collisions and a similar ratio of charged particles with $Z = 1$ and $Z = 2$ is seen by G.J. Kunde [47] in 100A·MeV Au+Au collisions.

The clear difference in energy as well as in total yield clearly favours the positioning of such a detector at the forward hemisphere. In the insert, the dependence of the multiplicity for light charged particles (again for $Z = 1$) is shown for impact parameters $b \le b_{\rm max} \le 14$ fm integrated over the full solid angle (dots) and integrated over a lab. emission-angle window of $10^\circ < \vartheta_{\rm lab} < 40^\circ$ (squares). It is evident that ∼50% of the total number of emitted protons still will be detected in a multiplicity detector (MD) system of which the acceptance is limited to the reduced angular window. Moreover the lab-energies of these protons are high enough to set up the MDs detached from the target vacuum, propagating the protons through an air gap, without significant loss of efficiency. Positioning the electron spectrometer in the backward hemisphere limits the background by heavy, highly ionizing charged particles to practically only pions and protons (see sect. 4.3.2).

3 Spectrometer design

3.1 Lepton detection technique

Leptons in the energy range of several tens of MeV are minimum ionizing particles ($\Delta E/\Delta x$ <5 keV/cm in air see, *e.g.*, fig. 6b). However, due to their comparatively small masses, they are subject to substantial angular scattering when they pass through matter. Their detection

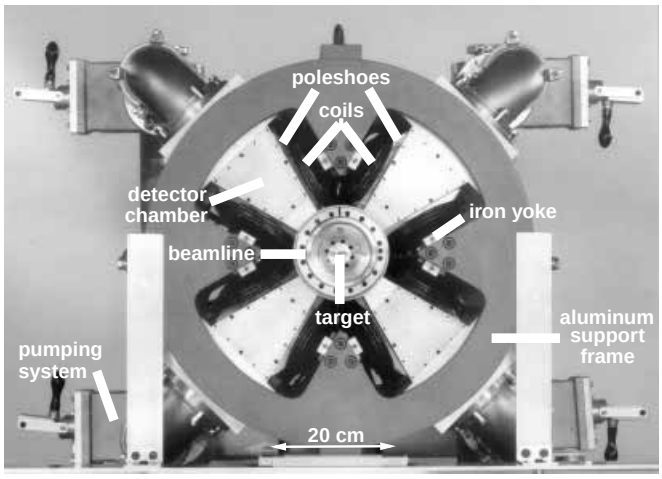

Fig. 5. 4-gap toroidal magnetic system with detector vacuum chambers and target chamber assembled.

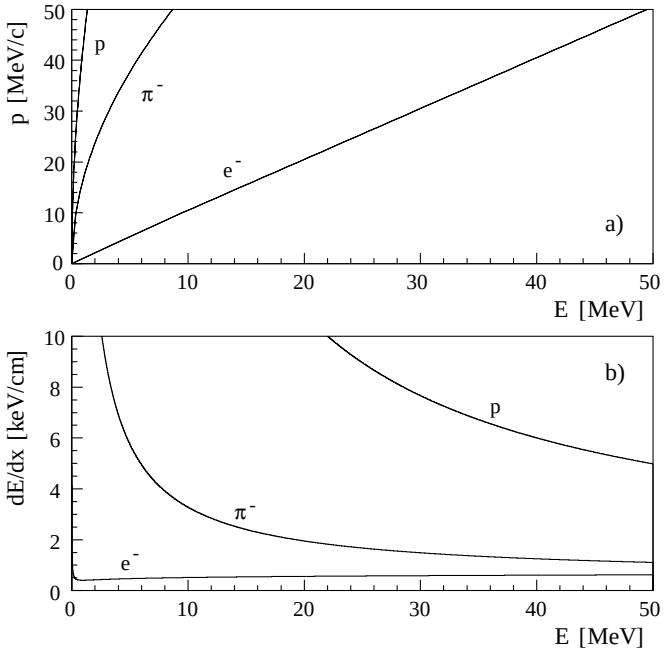

Fig. 6. The particle's trajectories inside the gap are characterized by their K value and hence by their momentum. (a) displays the momentum of protons, pions and electrons as a function of their kinetic energy. (b) shows their energy loss in 100 mbar isobutane as a function of the kinetic energy.

thus either calls for large-volume calorimeter systems of high granularity for full energy detection or minimum-distorting detection techniques for path reconstruction with low-mass/low-Z tracking detectors in combination with a magnetic field for the determination of the lepton momenta.

Dynamically induced atomic lepton emission exhibits exponential spectral shapes (see fig. 1). Therefore the energy resolution is of minor importance compared to the lepton selectivity and the total detection efficiency. By using path reconstruction *inside* a magnetic field with position-sensitive multi-wire-proportional counters (MWPC), a compact "large-solid-angle" lepton spectrometer can be constructed. Basically, the momentum resolution is limited by the path distortion due to small angular scattering of the leptons in the detector gas and foils of the system. By minimizing the number of foils and low gas pressures (LP-MWPC) the latter influence can be substantially reduced.

3.2 Magnetic system

A magnetic system, which ideally fulfills all demands, is a toroidal magnetic configuration with a $1/r$ field geometry. This geometry is utilized in iron-free ORANGE-type spectrometers with normal conduction coils used at Coulomb barrier heavy-ion collisions for energies below a few MeV [19,22,48]. In the 10 to 100 MeV range an iron enforced magnet like a Kofoed-Hansen–type spectrometer [49] can be applied. For further increased lepton energies super conducting versions of toroidal type spectrometers are used [50]. A toroidal assembly provides the largest possible acceptance if spectrometer and beam axis coincide. The $1/r$ field dependence then has the advantage to guide the intense low-energy leptons of highest intensity of the exponentially decreasing δ-electron spectrum out of the magnetic field (cycloidal trajectories) in contrast to homogeneous fields where, to first order, these leptons are caught on stationary circular orbits. With a limited number of coils and with iron gaps the $1/r$-geometry of the field distribution is reached only approximately. In fig. 5 an example is given for a 4-gap system. This system has been chosen to pursue first exploratory experiments. It has an outer diameter of ≈ 70 cm and a length of ≈ 50 cm. The details of this instrument will be given elsewhere.

Performing ray tracing *inside* the magnetic field is the natural solution for obtaining large momentum band acceptance, and to minimize the effective track lengths in the detector gas volume causing multiple scattering. The maximum length of a lepton trajectory has been chosen to be 400 mm (200 mm effective length). The magnetic system has a diameter of 660 mm. Each 30° field gap has a length of 430 mm and a (radial) width of 250 mm. For the lepton energy range investigated here a magnetic field at the inner pole edge of $B_{\max} \approx 0.5$ T is required.

3.3 Path reconstruction

Two pieces of information are principally sufficient to reconstruct the energy of leptons emitted from the target: The angle of emission and one second point of the trajectory. Unfortunately in the given environment, no detector can be mounted in the direct vicinity of the target to directly measure the emission angle of the leptons without distortion by the magnetic field. Such a detector would be exposed to highly ionizing particles (slow p^+, d^+, α, $\pi^\pm$) from the target which will inevitably damage the detector. Due to their much larger momenta even at low velocities (see fig. 6) these particles pass the field gap practically on

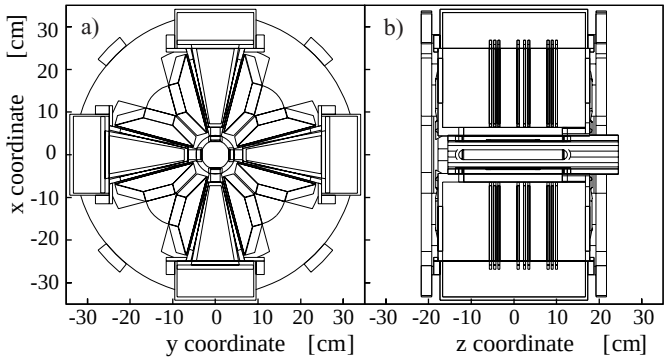

Fig. 7. a) Transversal and b) longitudinal cut through the proposed spectrometer set-up shown in fig. 5 as modelled for the GEANT simulations.

straight trajectories, so that the first detector has to be placed inside the magnetic gap as close to the target as possible but at a position where no straight trajectories from the target can hit the detector. As shown in fig. 6a only extremely low-energetic pions ($E_{\pi^-} \leq 10$ MeV) have substantially curved trajectories and therefore cannot be distinguished from electrons with energies below 50 MeV. However, at these energies, pions are no longer minimum ionizing particles and can clearly be separated from leptons by means of their substantially higher energy loss in the detectors (see fig. 6b).

The second detector is positioned inside the magnetic field to achieve the best dispersion for the trajectories. Together with the information from the first detector a lepton path can be reconstructed *if it has emerged from the target.*

It is meaningful to add a third MWPC-detector to the assembly. This detector allows to reduce the random trigger rate by rejecting invalid "hit-pattern combinations" of the three detectors like straight-line trajectories or those, that do not originate in the target. For this purpose the position information of all detectors has to be processed in a fast pattern recognition and trigger logic (MUEK [51, 52]).

In addition to this, the third detector provides redundant information on a given trajectory (identical information can be deduced from different sets of two out of three detectors). This allows to determine and on-line control the detector efficiency. This is important for long-run experiments with detectors with dynamic gas flow.

3.4 Lepton detectors

In a separate study low-pressure multi-wire proportional counters (LP-MWPC), especially designed for lepton detection in the energy range above 5 MeV have been developed [53,54]. They allow lepton detection at full efficiency ($\varepsilon = 1$) at pressures >100 mbar of iso-butane as detector gas at an active depth of 10 mm resulting in low straggling of the electrons. This corresponds to the detection at a statistical level of approximately 5 primary ionizations [55,56] with gas amplifications as high as 4×10^6 [53,54].

In test runs (see sect. 5) the LP-MWPC were safely operated at a gas pressure of 200 mbar for lepton energies as low as 5 MeV [53,54] at an entrance window thickness of 1.4 mg/cm^2 polyimide film. For higher lepton energies of 20 to 50 MeV with less angular straggling the detectors will be operated at a pressure of 400 mbar. This will allow to further reduce the gas amplification so that highly ionizing pions will not cause local breakdowns of the detectors.

4 GEANT simulations of the spectrometer design

4.1 Determination of spectrometer parameters

As trajectories in toroidal magnetic fields can only be described analytically by assuming ideal $1/r$-field dependence, the determination of the properties of a given spectrometer assembly are best deduced by numerical calculations. In the first design step, a ray-tracing program has been developed to study various spectrometer geometries [57]. The program is modular such that any calculated or measured field map of a real spectrometer as well as additional conditions like detector resolution, angular straggling etc. can be linked. With this program we have developed the following spectrometer design. In order to account for secondary reactions in the mechanical elements of the set-up, the computer code GEANT [58] provided by CERN has additionally been used. The full geometric implementation of the 4-gap spectrometer designed in the first step by the GEANT preprocessor is displayed in fig. 7a-b.

In this arrangement, three MWPC detectors are installed in each of the four magnetic-field gaps. Each MWPC is oriented perpendicular to the spectrometer axis and consists of three wire planes (1 anode, 2 cathodes). The wire planes are spanned onto 5 mm thick epoxy frames (NEMA G10, Stesalit®). In the simulation only the massive frames are taken into account whereas the wires (10 μm anode, 50 μm cathodes) are neglected. In this design, beam and spectrometer axis coincide. The lepton source (target) is located on axis at $z = -12.0$ cm (see fig. 7b).

Start parameters for the simulations are the emission angles of the leptons in cylindrical coordinates and their momenta in terms of their K values [59]

$$K = \frac{p}{qB_{\max}} \cdot \frac{1}{r_{\min}} = \frac{\rho}{r}\Big|_{B=B_{\max}, r=r_{\min}} . \qquad (1)$$

Here p is the particle's momentum, q its charge, $B_{\max}$ the field strength at the inner pole-face edge at a distance $r_{\min}$ with respect to the beam axis for the maximal setting of the spectrometer current. ρ is the radius of curvature of the trajectory. As a result, the coordinates of hit points in all detectors are generated. The simulation data shown in this paper are results of GEANT calculations, where the 4-gap spectrometer was implemented (see also fig. 11).

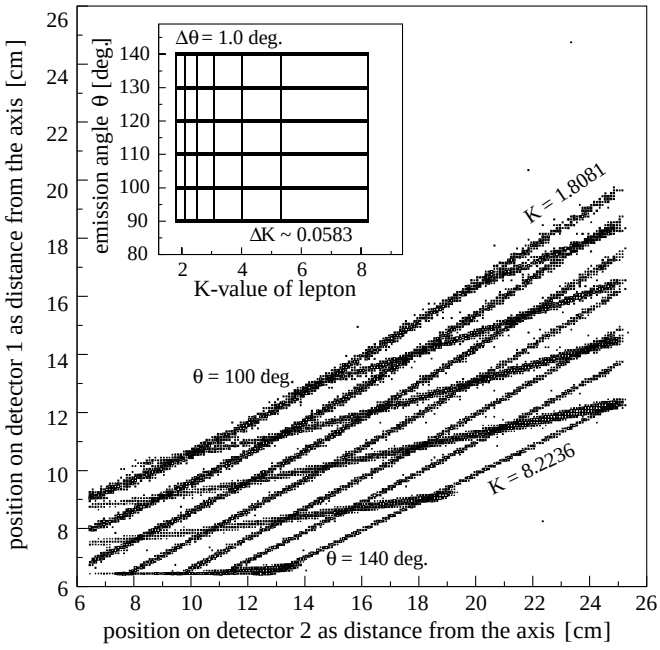

Fig. 8. GEANT calculations for the expected hit positions for electrons (radial distance r with respect to the beam axis) on the detectors 1 and 2. In order to better elucidate the transformation properties the discrete θ/K-event distribution displayed in the insert has been chosen as input pattern for the simulations.

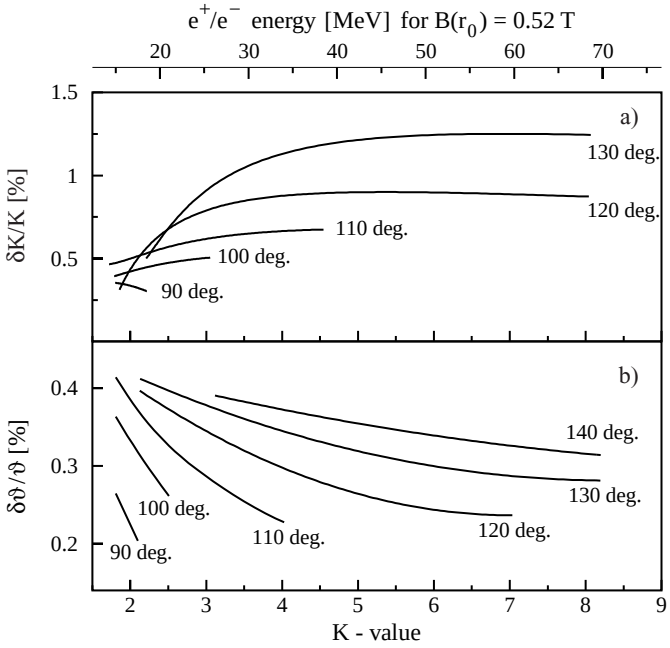

Fig. 9. a) Momentum and b) angular resolution as a function of the K value defined in eq. (1).

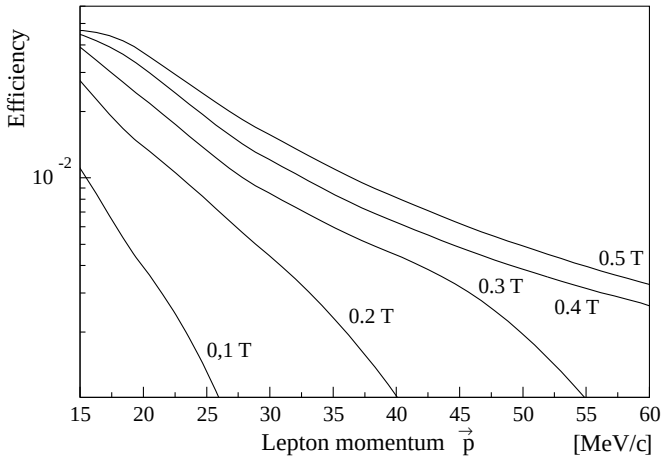

Fig. 10. Spectrometer efficiency as as function of the lepton momentum and various magnetic-field settings.

To demonstrate the transport properties of the 4-gap set-up, in fig. 8 a simulated scatter plot of the position correlation between two detectors for a magnetic-field setting of $B_{\max} = 0.52$ T is displayed. The detector coordinates are given in centimeters from the axis. A target spot size of $\delta z = 1$ mm and $\delta r = 0.5$ mm and a detector resolution of 1 mm has been chosen. As starting condition a discrete two-dimensional lepton distribution $\mathrm{N}(\vartheta_{\mathrm{lab}}, \mathrm{K}_{\mathrm{lepton}})$ as indicated in the insert has been used.

In fig. 9 the angular and momentum resolutions ($\delta\theta/\theta$, $\delta K/K$) are given as a function of the K value. For better understanding a lepton-energy scale (upper scale) is also added. This scale, unlike the K-representation, depends on the actual field setting and is given for $B_{\max}(r_{\min}) = 0.52$ T.

Angular as well as momentum resolution depend on the one-dimensional resolution δr for the radial track position, *i.e.* the position resolution of the detectors. For the results given in fig. 9 a position resolution of $\delta r = 1$ mm was assumed. The upper limits of $\delta\theta/\theta < 1.25$ and $\delta K/K < 0.4$ correspond to the kinematical broadening of monoenergetic leptons emitted with a cone of ± 2.5 deg into the backward hemisphere from a source moving with the CM-velocity of a 60 A·MeV Pb+Pb reaction. Therefore the proposed spectrometer system can excellently be applied for the measurement of lepton emission in heavy-ion collisions at intermediate and higher collision energies with exponentially decreasing or moderately structured spectra.

In fig. 10 the geometric efficiencies are given as a function of the lepton momentum for various field settings of the system. For an isotropic emission within the lab. system the geometric efficiency is also the detection efficiency if a detector efficiency of $\varepsilon = 1$ is assumed.

4.2 Optimization of the target geometry

In contrast to a focusing instrument, the tracking spectrometer offers some freedom in choosing the position of the target. For the present 4-gap spectrometer the accepted angular and energy windows are rather insensitive to the axial target position —they remain essentially unchanged for axial positions varying within ±15 mm—

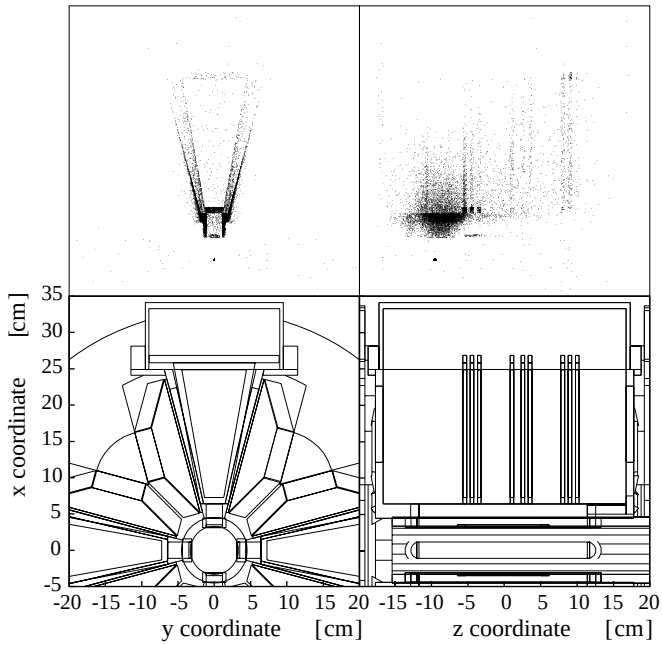

Fig. 11. GEANT simulation of γ-ray induced events. Top: front (left) and side view (right) scatter plots of the origins of triple hits in one sector of the spectrometer. The target has been positioned at $z = -9.5$ cm. Bottom: corresponding window of the spectrometer set-up for visualization of the components. For a full view of the spectrometer see fig. 7.

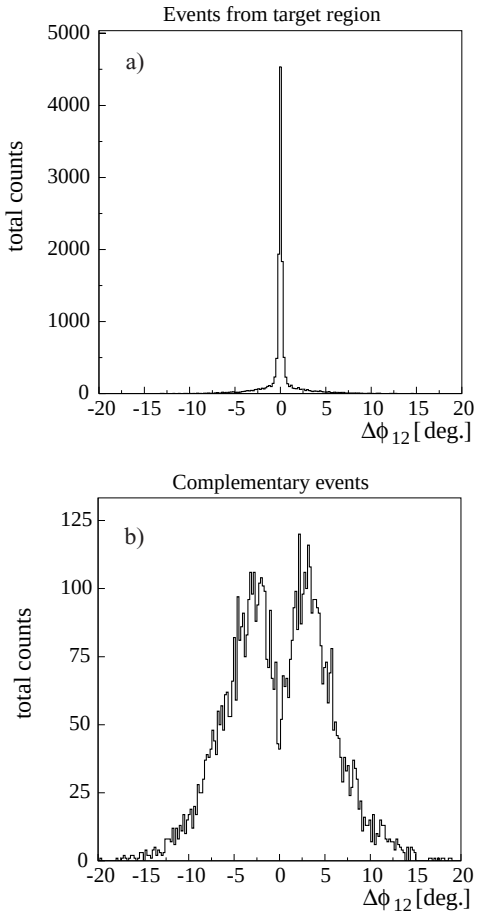

Fig. 12. Differences $\Delta\phi_{12}$ of the azimuthal angle of "target" (a) and "spectrometer" (b) events.

but vary with a target displacement in radial direction. Thus using a vertically thin, but axially extended target will improve the ratio $V = N(\text{primary})/N(\text{secondary})$ of leptons created in the target in primary ion-atom reactions over those created by secondary processes. For instance, by using a funnel-shaped target of 30 mm length and 0.03 mm thickness in the 4-gap spectrometer a gain in V of about 25 can be achieved compared to a conventional 1 mm thick planar target. If an extended target is used, a third MWPC detector is necessary to reconstruct the lepton's path.

4.3 In-beam characteristics of the spectrometer

4.3.1 Suppression of γ-radiation

A major source of background events is external conversion (EPC) of γ-radiation in the target and the material of the set-up.

Extrapolated data from intermediate-energy heavy-ion collisions [43,60,61] has been used as input for the simulation. To first order the shapes of these spectra are exponentially decreasing by approximately three orders of magnitude within an energy range of 0–200 MeV. This results in negligible contributions from higher energies. A cut-off was therefore introduced at 200 MeV. A total number of $1.2{\times}10^7$ γ-rays following all secondary charged particle events from interactions with spectrometer materials have been tracked.

Figure 11 illustrates the production of secondary events. In the "GEANT-views" of the spectrometer (front and side view) the origins of those secondary particles are shown, that traversed all three MWPC planes. The expected strong lepton production at the spectrometer entrance is obvious. A non-negligible amount of events is also created at the massive frames ($5{\times}5$ mm^2 Stesalit®) of the MWPC detectors. Even at the second and third MWPC-plane secondary electrons/positrons are created that trespass all three detectors, whereas secondaries created in the chamber walls and in the yoke are mainly restricted to the target area. It has already been pointed out (sect. 4.2), that EPC events from the target itself can be minimized by using pencil-like or cone-shaped targets.

For the simulations given here, a massive spherical lead target of 1 mm diameter without special support and an efficiency of $\varepsilon = 1$ for all three MWPCs has been assumed. From $1.2{\times}10^7$ started γ-rays a number of 6586 events (secondary charged particles) have traversed all three MWPC-planes. This represents a γ-ray suppression factor of $N(\gamma)_{\text{valid}}/N(\gamma)_{\text{actual}} = 5.5 \times 10^{-4}$.

The analysis further shows, that events, originating in the target or, more general, on axis, result in tracks that are detected with only small deviations of the azimuthal emission angle ϕ_{lab} in all three MWPC detectors

Table 1. Characteristic data of the 1-gap test spectrometer.

Number of gaps	1
Outer diameter	660 mm
Depth	435 mm
$B_{\max}$	0.6 T
Radius $r_{B_{\max}}$	63 – 65 mm
Radius of det. chamb. entrance	55 mm
max. ϕ accept./gap	$\pm$15 deg.
$\theta_{\min}$	85 – 90 deg.
$\theta_{\max}$	130 – 135 deg.
max. K value	≈ 5
max. lepton energy	up to 50 MeV
$\Delta E/E$	47 %
$\Delta p/p$	4–6 %

($\Delta\phi_{ij}^{\rm lab} = \Delta\phi_i^{\rm lab} - \Delta\phi_j^{\rm lab} < \pm 1°$). In contrast to this, tracks of secondary events exhibit a clear out-of-plane behaviour (fig. 12).

Assuming in first order a Gaussian distribution for the "target events", approximately 78 % of all events fall within a window of $\Delta\phi_{\rm lab} = 0° \pm 0.65°$. By applying the same window for the analysis of the "spectrometer events" approximately 91.8 % will be rejected, improving the γ-ray suppression factor further by approximately one order of magnitude. Furthermore, the energies of the remaining events (8.2%) are peaked around 20 MeV with a steep decline towards higher values forming an exponentially decreasing background which can further be reduced by the final track analysis.

4.3.2 Hadronic background

As has been pointed out in sect. 2.1 the hadronic background mainly consists of pions and protons.

Comparing spectra 4a and 4b it becomes obvious that protons are already kinematically suppressed in the angular acceptance window of the spectrometer.

Transforming mean energy distributions $\mathrm{d}E/\mathrm{d}\theta_{\rm cm}$, measured by Kunde [47] for central 100 A·MeV Au+Au collisons, into the laboratory frame of a 60 A·MeV Pb+Pb collision system and assuming isotropic emission in the centre-of-mass frame a backward-forward asymmetry of $I_{\rm backw.}/I_{\rm forw.} = 0.2$ can be deduced.

Taking the data of ref. [47] an average proton rate of 1 per detector gap has to be expected for central collisions. This number has to be compared to an expected rate of atomic electrons in the order of 10^{-3} per central collision.

From these considerations it is evident that these background events have to be suppressed. In the spectrometer design this is achieved by positioning the detectors in such a way that straight trajectories traversing all three detector planes are excluded. This reduces the background to only chance coincidences between protons and leptons. In order to separate leptons and protons in those events, multihit capability is necessary. This will be realized by single-wire/group-wire readout of the detector information into a fast pattern recognition logic.

Compared to the number of protons the rate of pions can be neglected. As already shown in sect. 1, systematic measurements at various beam energies will allow to separate lepton contributions originating from π^0-decay. As written in section 3.3 extremely low-energetic pions ($E_{\pi^\pm} \leq 10$ MeV) can be separated by their higher energy loss in the detectors. Furthermore the polarity of the magnetic field selects the charge state of a particle so that trajectories of pions with complementary charge will be rejected by the path analysis. For high energetic pions with straight trajectories, the same method of suppression applies as for protons.

5 Tests of the spectrometer design

5.1 The 1-gap prototype spectrometer

In order to test the idea of path reconstruction in an inhomogeneous field in low-pressure (LP-) MWPC detectors, a 1-gap prototype spectrometer has been built already at an early stage of the study. The basics of its construction are essentially the same as for the proposed 4-gap spectrometer.

The parameters of this spectrometer are given in table 1. Two differences between both set-ups are worth mentioning here:

– A still markable field exists on the axis of the asymmetric 1-gap set-up, compared to a symmetric field configuration like in the 4-gap set-up, where the field on axis is zero by definition. The field on the axis of the 1-gap spectrometer is mainly generated at the expense of a reduced maximum field strength in the entrance region of the gap. This effect cancels to first order, but nevertheless was fully taken into account for the path reconstruction of the experiment, by implementing the measured field distribution.

– In order to limit the number of readout channels for the position determination a delay-line read-out concept was employed. Yet at the given background of γ- and particle radiation in this experiment, the detectors could not be operated at voltages giving sufficient amplification for the delay line read-out to achieve full efficiency. A triple coincidence trigger had to be implemented to reduce the high rate of singles events. The total efficiency thus was reduced to $\varepsilon < 0.01$ (and only spectral shapes could be analyzed). However, it was verified that the efficiency was constant in time and independent of the magnetic field setting. No such difficulties will arise if a single wire read-out is implemented.

5.2 The test measurement

The 1-gap prototype spectrometer has been used to investigate the β-decay of ^{12}B, produced by the reaction ^{11}B(d,p)^{12}B ($E_{\max} = 13.4$ MeV, $\tau_{1/2} = 27$ ms). The measurements were carried out at the 2.5 MV van de Graaff

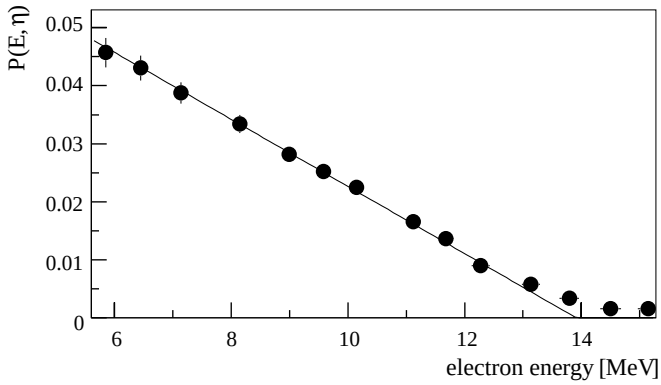

Fig. 13. Fermi plot of the ^{12}B β-decay obtained from test measurements with a prototype 1-gap spectrometer.

accelerator of the institute. The experiment was designed to simulate a heavy-ion in-beam environment by selecting a light collision system with various high-Q-value reaction channels ($Q \leq 20$ MeV).

The crucial test is the reconstruction of the lepton spectrum from the hit positions given by the three LP-MWPC at a given magnetic field setting. In fig. 13 the resulting spectrum is plotted in its Fermi representation. The data points result from six independent measurements at different settings of the magnetic field, normalized by the numbers of incident projectiles. No further normalization has been applied. The very good agreement in spectral shape and the *correct* reconstruction of the β-spectrum is evident. At energies below 5 MeV the reconstruction increasingly fails. This is mainly given by multiple scattering in the entrance foil and detector gas.

6 Conclusion

The spectroscopy of dynamically emitted atomic leptons from close intermediate-energy heavy-ion collisions is expected to serve as "atomic clock" for the early stage of the nuclear collision. In this particularly interesting collision-energy range, cooperative processes are predicted to play an important role for the meson production.

In this study we investigated the possibilities for a spectroscopy of light, minimum ionizing particles in the energy range from 10 to 50 MeV. In order to extract details of the nuclear collision from the experimentally measured lepton spectra, the data have to be compared to model calculations. Predictions on the cross-sections for the emission of dynamic atomic electrons/positrons from close Pb+Pb collisions at 60 A·MeV are given within an adiabatic atomic model [31]. The extrapolation of this model, which is very successful at Coulomb-barrier energies, into the regime of intermediate energies is still controversially discussed and has to be tested by dedicated experiments first.

Here, we introduce a spectrometer concept, where the leptons are analyzed by means of path reconstruction in windowless, low-pressure multiwire proportional counters inside a toroidal magnetic field. In an experiment the spectrometer will be positioned at the backward hemisphere, avoiding the outnumber of heavy reaction products from a close collision at intermediate energies. Using inverse kinematics or a symmetric collision system, these products are mainly directed into the forward hemisphere. In order to characterize the impact parameter of the nuclear collision, a highly segmented multiplicity detector will be supplemented at the forward hemisphere.

In the course of this study, extended Monte Carlo simulations have been carried out to derive and optimize the spectrometer parameters and to investigate the influence of background events from the nuclear reaction. Special emphasis has been laid on an optimal suppression of nuclear γ-radiation. The final design has been tested in a 1-gap prototype spectrometer utilizing the nuclear reaction ^{11}B(d,p)^{12}B. In this experiment, the lepton detection technique, the track reconstruction as well as a sufficient suppression against a realistically strong background of γ-radiation and heavy charged particles was verified.

The authors like to thank M. Waldschmidt and H. Stelzer at IKF for valuable discussions and suggestions, J. Reinhardt, at the Institut für theoretische Physik der Universität Frankfurt (UFTP), for several calculations and discussions and G. Peilert, J. Konopka and W. Greiner also at UFTP for the RQMD simulation data. One of the authors, K.A. Müller, is grateful for support by the Graduiertenkolleg Schwerionenphysik der Deutschen Forschungsgemeinschaft (DFG). This project was supported by Bundesministerium für Bildung und Forschung (BMBF) under contract No. 06 OF 474, Hessisches Ministerium für Wissenschaft und Kunst (HMWK) and Gesellschaft für Schwerionenforschung (GSI).

References

1. J. Stroth, H. Backe, M. Begemann-Blaich, K.Bethge, H. Bokemeyer, M. Dahlinger, W. Konen, P. Kosmadakis, S. Mojumder, P. Senger, K.E. Stiebing, Z. Phys. A **357**, 441 (1997).
2. H. Backe, P. Senger, W. Bonin, E. Kankeleit, M. Krämer, R. Krieg, V. Metag, N. Trautmann, J.B. Wilhelmy, Phys. Rev. Lett. **50**, 1838 (1983).
3. R. Krieg, E. Bozek, U. Gollerthan, E. Kankeleit, G. Klotz-Engman, M. Krämer, U. Meyer, H. Oeschler, P. Senger, Phys. Rev. C **34**, 562 (1986).
4. M. Krämer, B. Blank, E. Bozek, E. Kankeleit, G. Klotz-Engmann, C. Müntz, H. Oeschler, M. Rhein, Phys. Lett. B **201**, 215 (1988).
5. M. Rhein, R. Barth, E. Ditzel, H. Feldmeier, E. Kankeleit, V. Lips, C. Müntz, W. Nörenberg, H. Oeschler, A. Piechaczek, W. Polai, I. Schall, Phys. Rev. Lett. **69**, 1340 (1992).
6. J. Reinhardt, V. Oberacker, B. Müller, W. Greiner, G. Soff, Phys. Lett. B **78**, 183 (1978).
7. J. Reinhardt, B. Müller, W. Greiner, G. Soff, Phys. Rev. Lett. **43**, 1307 (1979).
8. G. Soff, J. Reinhardt, B. Müller, W. Greiner, Z. Phys. A **294**, 137 (1980).
9. G. Soff, J. Reinhardt, W. Greiner, Phys. Lett. A **83**, 158 (1981).

10. J. Reinhardt, B. Müller, W. Greiner, Phys. Rev. A **24**, 103 (1981).
11. J. Reinhardt W. Greiner, in *Heavy Ion Science*, edited by D.A. Bromley, Vol. **5** (Plenum Press, New York, 1985) pp. 3–138.
12. J. Reinhardt, B. Müller, W. Greiner, G. Soff, Z. Phys. A **292**, 211 (1979).
13. G. Soff, J. Reinhardt, B. Müller, W. Greiner, Phys. Rev. Lett. **43**, 1981 (1979).
14. U. Müller, G. Soff, T. de Reus, J. Reinhardt, B. Müller, W. Greiner, Z. Phys. A **313**, 263 (1983).
15. S. Mojumder. PhD thesis, Universität Frankfurt/Main (published as GSI-Report-90-12, 1990).
16. K. Sakaguchi, PhD thesis, Universität Frankfurt/Main (published as GSI-Report-90-05, 1990).
17. P. Salabura, PhD thesis, Universität Frankfurt/Main (published as GSI-Report-90-06, 1990).
18. D. Kraft, PhD thesis, Universität Frankfurt/Main, Institut für Kernphysik, IKF-D574 (1994).
19. P. Senger, H. Backe, M Begemann-Blaich, H. Bokemeyer, P. Glässel, D. v. Harrach, M. Klüver, W. Konen, K. Poppensieker, K. E. Stiebing, J. Stroth, K. Wallenwein, in *NATO ASI Series B: Physics*, *Physics of Strong Fields*, edited by W. Greiner, Vol. **153** (Plenum Press, New York, 1987) p. 432.
20. P. Salabura, A. Balanda, H. Bokemeyer, K. Sakaguchi, K.E. Stiebing, Acta Phys. Pol. B **26**, 939 (1995).
21. E. Kankeleit, U. Gollerthan, G.Klotz, M. Kollatz, M. Krämer, R. Krieg, U. Meyer, H. Oeschler, P. Senger, Nucl. Instrum. Methods A **234**, 81 (1985).
22. E. Berdermann, F. Bosch, P. Kienle, W. Koenig, C. Kozhuharov, H. Tsertos, S. Schuhbeck, S. Huchler, J. Kemmer, A. Schröter, Nucl. Phys. A **488**, 683c (1988).
23. J. Reinhardt W. Greiner, Rep. Prog. Phys. **40**, 219 (1977).
24. J.S. Greenberg P. Vincent, in *Heavy Ion Science*, edited by D.A. Bromley, Vol. **5** (Plenum Press, New York, 1985) pp. 141–421.
25. W. Greiner, B. Müller, J. Rafelski, *Quantum Electrodynamics of Strong Fields* (Springer Verlag, Berlin, 1985).
26. U. Müller G. Soff, Phys. Rep. **246**, 101 (1994).
27. W. Henning. Nucl. Phys. A **538**, 637c (1992).
28. J. Theis, J. Reinhardt, B. Müller, J. Phys. B: Atom. Molec. Phys. **12**, L479 (1979).
29. T. de Reus, J. Reinhardt, B. Müller, U. Müller, G. Soff, W. Greiner, Z. Phys. A **321**, 589 (1985).
30. T. de Reus, J. Reinhardt, B. Müller, W. Greiner, Phys. Lett. B **169**, 139 (1986).
31. T. de Reus, U. Müller-Nehler, G. Soff, J. Reinhardt, S. Graf, B. Müller, W. Greiner, Phys. Rev. C **40**, 752 (1989).
32. Th. de Reus, PhD thesis, Universität Frankfurt (1987, published as GSI Report-87-8).
33. H. Heckwolf, E. Grosse, H.Dabrowski, O. Klepper, C. Michel, W.F.J. Müller, H. Noll, C. Brendel, W. Rösch, J. Julien, G.S. Pappalardo, G. Bizard, J.L. Laville, A.C. Mueller, J. Peter, Z. Phys. A **315**, 243 (1984).
34. W. Cassing, V. Metag, U. Mosel, K. Niita, Phys. Rep. **188**, 363 (1990).
35. J. Ritman *et al.*, Phys. Rev. Lett. **70**, 533 (1993); Phys. Rev. Lett. **70**, 2659(E) (1993)
36. H. Emling, Progr. Part. Nucl. Phys. **33**, 729 (1994).
37. G.D. Westfall, J. Gosset, P.J. Johansen, A.M. Poskanzer, W.G. Meyer, H.H. Gutbrod, A. Sandoval, R. Stock, Phys. Rev. Lett. **37**, 1202 (1976).
38. J. Gosset, H.H. Gutbrod, W.G. Meyer, A.M. Poskanzer, A. Sandoval, R. Stock, G.D. Westfall, Phys. Rev. C **16**, 629 (1977).
39. R. Stock, Phys. Rep. **135**, 259 (1986).
40. The Particle Data Group, Phys. Rev. D **50**, 1196 (1994).
41. K.A. Müller, PhD thesis in preparation, Universität Frankfurt/Main.
42. G. Martinez *et al.*, Phys. Lett B **349**, 23 (1995).
43. V. Metag, Nucl. Phys. A **488**, 483c (1988).
44. N.P. Samios, Phys. Rev. **121**, 275 (1961).
45. G. Fai J. Randrup, Comp. Phys. Com. **42**, 385 (1986).
46. P.M. Milazzo, G. Vannini, M. Azzano, D. Fontana, G.V. Margagliotti, P.F. Mastinu, R. Rui, F. Tonetto, N. Colonna, A. Botvina, M. Bruno, M. D'Agostino, M.L. Fiandri, F. Gramegna, I. Iori, A. Moroni, J.D. Dinius, S. Gaff, C.K. Gelbke, T. Glasmacher, M.J. Huang, G.J. Kunde, W.G. Lynch, L. Martin, C.P. Montoya, H. Xi, Phys. Rev. C **58**, 953 (1998).
47. G.J. Kunde, PhD thesis, Universität Frankfurt/Main (1994).
48. E. Moll E. Kankeleit, Nukleonik **7**, 180 (1965).
49. O. Kofoed-Hansen, J. Lindhard, O.B. Nielsen, Mat. Fys. Medd. Dan. Vid. Selsk. **25**, 3 (1950).
50. R. Schicker, A. Brenschede, K. Garrow, H. Schön, A. Balanda, H. Bokemeyer, J. Friese, W. Karig, P. Kienle, W. Koenig, W. Kühn, F. Lefèvre, V. Metag, G. Roche, P. Salabura, A. Schröter, J. Stroth, H. Tsertos, Nucl. Phys. A **380**, 586 (1996).
51. G. Lambrinidis, Master's thesis, Universität Frankfurt/Main, Institut für Kernphysik, IKF-D567 (1994).
52. G. Lambrinidis, K.E. Stiebing, K.A. Müller, O. Fröhlich, G. Rüschmann, K. Bethge, Universität Frankfurt/Main, Institut für Kernphysik, Annual Report IKF-D 54 (1993). p. 74.
53. A. Müller, J. Peter, K. Bethge, S. Mojumder, K.E. Stiebing, H. Bokemeyer, H. Folger, E. Grosse, P. Senger, A. Balanda, GSI-Report, GSI 88-1, 306 (1988).
54. A. Müller, Master's thesis, Universität Frankfurt/Main, Institut für Kernphysik, IKF-D397 (1988).
55. F. Sauli, *Principles of Multiwire Proportional Drift Chambers*, CERN-77-09 edition (1977).
56. Th. Ferbel (Editor), *Contributions of F. Sauli K. Kleinknecht*, in *Experimental Techniques in High Energy Physics* (Addison-Wesley, Menlo Park, 1987).
57. J. Peter, Master's thesis, Universität Frankfurt/Main, Institut für Kernphysik, IKF D-396 (1988).
58. R. Brun, F. Bruyant, M. Maire, A.C. McPherson, P. Zanarini, *GEANT – Detector Description and Simulation Tool*, CERN DD/EE/84-1 edition (1987), CERN Program Library Long Writeup W5013.
59. K. Siegbahn (Editor), *Alpha-, Beta- and Gamma-ray Spectroscopy*, Vol. **1** (North-Holland Publishing Company Amsterdam, 1979).
60. E. Grosse, P. Grimm, H. Heckwolf, W.F.J. Müller, H. Noll, A. Oskarsson, H. Stelzer, W. Roesch, Europhys. Lett. **2**, 9 (1986).
61. A. Schubert *et al.*, Phys. Rev. Lett. **72**, 1608 (1994).